Science of the Total Environment 890 (2023) 164363

Contents lists available at ScienceDirect

Science of the Total Environment

journal homepage: www.elsevier.com/locate/scitotenv

Suspended sediments mediate microplastic sedimentation in unidirectional flows

Mirco Mancini [a], Teresa Serra [b,*], Jordi Colomer [b], Luca Solari [a]

[a] Department of Civil and Environmental Engineering, University of Florence, Via S. Marta 3, 50139 Florence, Italy
[b] Department of Physics, University of Girona, Campus Montilivi, 17003 Girona, Spain

HIGHLIGHTS

- Sedimentation rates increased linearly as sediment concentration increased.
- Sedimentation rates of MP depended on the type of MP particles.
- Fast settling sediments scavenged MP to the bottom of the water column.
- In shallow water bodies, MP settle and accumulate near their source.

GRAPHICAL ABSTRACT

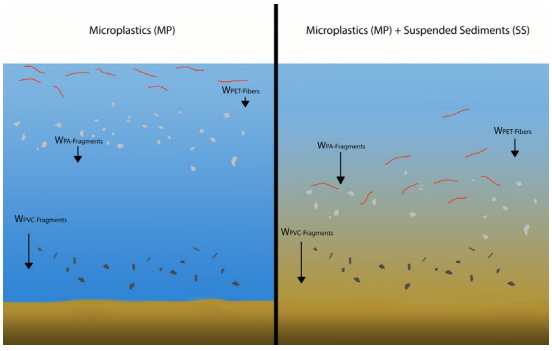

ARTICLE INFO

Editor: Damia Barcelo

Keywords:
Plastic fragments
Plastic fibers
Sediment interaction
Shallow aquatic system
Scavenging
Sedimentation rate

ABSTRACT

Microplastic particles (MP) are an emerging contaminant threatening many aquatic systems. Because of the sharp increase in plastic manufacture, the concentration of MP in natural ecosystems has grown dramatically. While it is known that when MP enter aquatic ecosystems they are transported and dispersed via different mechanisms (currents, waves, turbulence), the processes involved are still poorly understood. In the current study, the transport of MP by a unidirectional flow has been investigated in a laboratory flume. MP enter the system through a plume that can (or not) have suspended sediment. The interaction between MP and sediment was studied for three different MP particle types (Polyamide (PA) and Polyvinyl Chloride (PVC) fragments, and Polyethylene Terephthalate (PET) fibers), and four different sediment concentrations (0 g/l, 15 g/l, 30 g/l and 45 g/l). In all cases, sediment increased the vertical transport of MP to the bottom. The greater the sediment concentration, the greater the downward flux of MP. Sediment particles scavenged PA fragments downwards at the highest rate, followed by PET fibers and finally PVC fragments. These results indicate that a sediment particle-laden plume carrying MP may induce a differential settling of MP as they are advected. The scavenging of MP by sediments may result in sedimentation segregated patterns, with MP being found at shorter distances than expected for the case without sediment, therefore increasing the presence of MP near their contaminant sources.

1. Introduction

The plastics industry was founded 80 years ago and since then its production has grown exponentially (Streit-Bianchi et al., 2020). While the versatility and resistance of plastics make them suitable for a wide range of applications, the linear economy of the plastics, together with their durability, are causing a global environmental crisis as large amounts of plastic waste are ending up in ecosystems, ultimately endangering the flora and fauna (Colomer et al., 2019; Pinheiro et al., 2022). Meijer et al. (2021) found a 1.2 and 4.0 % probability of mismanaged plastic waste generated on land entering freshwater environments. The largest groups of non-

* Corresponding author.
E-mail address: teresa.serra@udg.edu (T. Serra).

http://dx.doi.org/10.1016/j.scitotenv.2023.164363
Received 28 March 2023; Received in revised form 17 May 2023; Accepted 18 May 2023
Available online 20 May 2023

fiber plastics are polyethylene (PE), polypropylene (PP), polyvinylchloride (PVC), while polyethylene terephthalate (PET) is the main material constituting fibers (Geyer et al., 2017).

In natural environments, plastic particles are degraded by UV light and mechanical abrasion (Sun et al., 2022), i.e., are decomposed into microplastic particles of <5 mm (MP). Seas and oceans are the final receptors of the macro- and microplastics (MPs), where their negative effects on marine life are strongly dependent on their concentration levels (Bergmann et al., 2015). As a result, many studies have focused on either quantifying plastic debris in the marine environment (Hidalgo-Ruz et al., 2012; Ivar Do Sul and Costa, 2014; van Cauwenberghe et al., 2013; Woodall et al., 2014), or on the behavior of plastic particles in fresh waters and their residence time in rivers (Besseling et al., 2017; Siegfried et al., 2017; van Emmerik et al., 2019) in an attempt to quantify plastic debris fluxes that are discharged from rivers into coastal and open waters.

Rivers are known to be major pathways to the ocean for MP debris, with larger MP abundance occurring in higher river discharges (Schmidt et al., 2018; Zhao et al., 2019). Experimental and modeling studies have been conducted to describe the spatial and temporal distribution of plastic particles via environmental systems. For example, Global Modeling highlighted the crucial role inland waters play in retaining and storing MPs. Some studies state riverbed sediments, riverbanks and floodplains can be long-term sinks for MPs (He et al., 2021; van Emmerik et al., 2022). Spatiotemporally explicit models consider advection, homo- and hetero-aggregation, biofouling, sedimentation, resuspension, and degradation of micro- and nanoparticles (de Klein et al., 2016) to determine the transport of MP (Wagner and Lambert, 2018) in aquatic systems. However, to be able to successfully apply spatiotemporally explicit models to various aquatic environments it is required to first advance the knowledge of the transport mechanisms and the particle-particle interactions. One of the fundamental parameters with which to describe the vertical transport of plastic particles in water environments, is their characteristic settling velocity (Ballent et al., 2013; Critchell and Lambrechts, 2016). The settling velocity of particles in natural waters (natural particles or MP particles) is expected to depend on both the physical properties of the particles (e.g., size, shape, and density) and the characteristics of the medium in which it is immersed (Dietrich, 1982). But not only this, the vertical transport of MP can be affected by several environmental conditions such as turbulence (Rahmani et al., 2022), interaction with other suspended particles (Liu et al., 2022), or salinity (Wang et al., 2023). Under high concentrations of inorganic (like sediment particles) and organic particles (like microalgae) in freshwater environments can produce heteroaggregation (i.e. formation of aggregates of different types of particles) (Besseling et al., 2017; Wang et al., 2021). Particle aggregation is governed by MP properties like size, shape, density, and aging (Kumar et al., 2021), as well as the physicochemical properties of the water (Yan et al., 2021). Some microscopic organic particles, like microalgae, can adhere to MP and modify their buoyancy (Lagarde et al., 2016). The aggregation timescale between MP and organic or inorganic particles requires long contact times of at least hours or days (Bakhteeva et al., 2023; Lagarde et al., 2016).

Shallow water environments such as floodplains, wetlands, intertidal zones, saltmarshes, or end of river courses represent areas where MP can accumulate (Pinheiro et al., 2022) and are recognized as likely hotspots where MP and other toxic substances can enter the systems via freshwater or sewage or directly via land-based activities (Huang et al., 2021; Ouyang et al., 2022; Sanchez-Vidal et al., 2021). Because they are totally or partially enclosed areas with low energy zones, stagnant water, low flow velocities and low channel slopes (Keddy, 2010), they enhance MP accumulation. Currents, flooding events and turbulence produced by wind promotes the presence of suspended sediments (Murphy and Voulgaris, 2006; Smoak et al., 2013) that are expected to be transported along with MP particles. However, to date, knowledge concerning the transport of MP in such transitional environments is limited (Helcoski et al., 2020), and the retention mechanism of MP and the time scales of MP processes, as well as the interaction with suspended sediment particles, remain unknown. In addition, the contribution floodplains, wetlands, lagoons, intertidal zones, saltmarshes, and generally shallow water areas make, is rarely taken into account in MP mass balance models.

In this work, we investigate the transport capabilities of a particle-laden (MP and sediment) plume in a simulated shallow water system under a unidirectional flow. Three of the most common MP are considered: Polyamide (PA) and polyvinyl chloride (PVC) fragments, and polyethylene terephthalate (PET) fibers. The main hypothesis are that sediment particles will enhance the sedimentation rate of MP in the water column and that the greater the sediment concentration the fastest the flux of MP particles to the bottom of the water column. In order to test these hypotheses, the interaction between sediment particles and MP is studied through flume experiments with different sediment and MP concentrations. The aim is to understand the MP distribution deposited at the bottom of shallow water systems dominated by advection.

2. Materials and methods

2.1. The flume

Experiments were carried out in a 500 cm × 40 cm × 50 cm laboratory flume. At the entrance of the flume, a honeycomb was used to straighten the flow produced at the inlet (Nepf et al., 1997), while at the outlet, an 18 cm high gate ensured a constant flow level. The flume had a storage tank that allowed the water to be recirculated using a pump with a valve that could control the flow in the flume. A 10 cm high platform measuring 258 cm along the base and 238 cm along the top was constructed and placed in the flume to create a shallow zone (Fig. 1); resulting in a water height (H) of 9 cm. The flow velocity was measured in the shallow zone using a laboratory Doppler velocimeter (ADV, 16 MHz, SonTek Inc.). Ten sampling points along the main axis of the flume (at x = 0 cm, 25 cm, 50 cm, 75 cm, 100 cm, 131 cm, 162 cm, 187 cm, 212 cm, and 237 cm) were considered. The ADV measured the three components of flow velocity at each sampling point employing a frequency of 50 Hz for 5 min at a single point situated 5 cm from the probe tip and with a sampling volume of 0.09 cm^3. This resulted in a set of 15,000 data points. The ADV was placed in the flume in a downward-looking configuration and connected to a PC with data acquisition software. The ADV was moved along the horizontal direction and then fixed at the measuring point. All measurements were taken at the center of the flume in the transversal direction (y = 0 cm, Fig. 1) and at 3 cm above the bottom in the testing area. The temporal mean velocity of the x-component at each position was calculated as the mean value of the 15,000 measurements. In the shallow zone, the flow velocity (u) in x -direction was constant, with a mean current velocity of 1.2 ± 0.2 cm/s. The Reynolds number of the flow in the flume ($Re = \rho uR / \mu = 2277$) was calculated assuming the characteristic diameter of the flume (R) as $R = (HL)^{0.5}$, where L is the width of the flume, ρ is the water density, and μ is the water viscosity, resulting in a transitional flow regime very close to the laminar regime.

2.2. Experimental procedure

Two sediment traps were situated at each of the ten different distances x along the main axis of the flume (at y = 10 cm and y = −10 cm), accounting for a total of twenty sediment traps (Fig. 1). Sediment traps consisted of glass boxes 5 × 5 cm large and 0.9 cm high, previously positioned at the bottom of the flume (Fig. 1). MP and sediment particles were injected separately to avoid interaction between them before entering the flume. For this purpose, two mixing tanks were used (Section C, Fig. 1). Sediments and MP were previously diluted in 2 l and 1 l of water, respectively. MP and sediments were injected into the water, with a total injection time that lasted approximately 2.5 min (Total discharge 0.02 l/s). This injection time was chosen because it was the time frame required for the plume of particles to reach the end of the shallow zone. The time steps for the head of the sediment and MP plumes passing through each sampling point were acquired. As soon as the plume of particles had reached the end of the shallow zone, a gate at the inlet of the flume was lowered and the

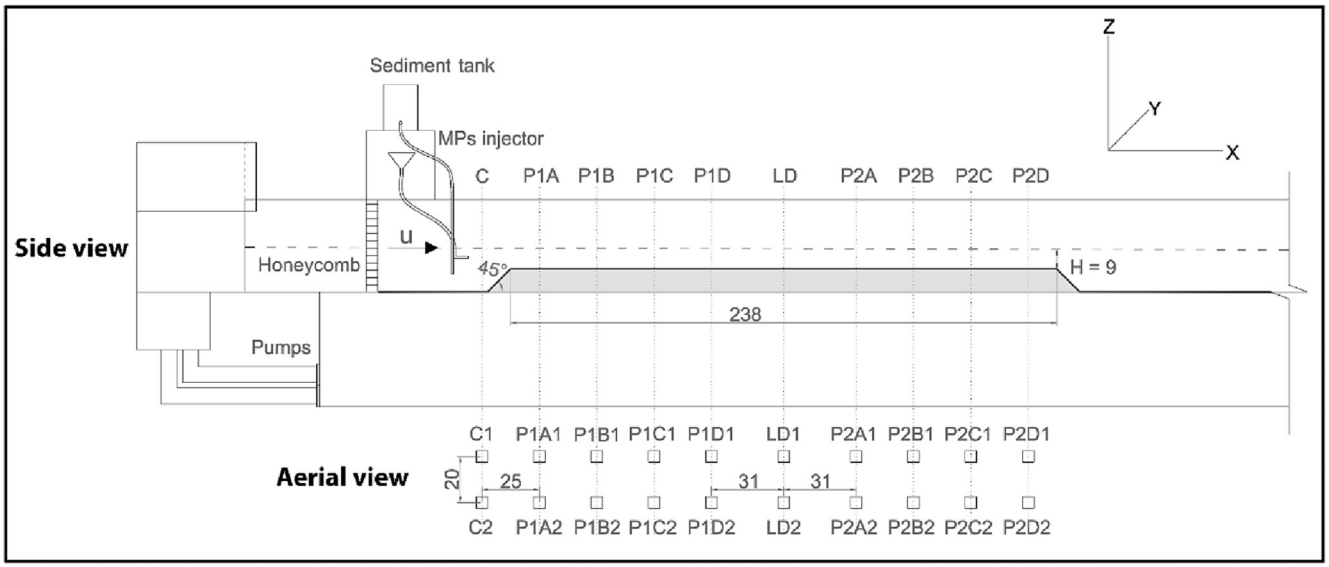

Fig. 1. Scheme of the experimental flume: Side and aerial views of flume with trap sampling positions (P1A to P2D). All measurements are in cm.

water remained in the section under study for 600 s so that particles could settle in the system. After this period, all sediment traps were covered with a lid and collected for analysis. The identical procedure was repeated for all experiments to reduce any variability. One of the experiments (see Table 1) was repeated three times to check for replicability. Experiments were performed separately for each type of MP (see Table 1 for all the runs carried out). Four sediment concentrations in the mixing chamber (C_{sed} = 0, 15, 30 and 45 g/l, Table 1) and three types of MP (PVC and PA fragments and PET fibers) were considered in the experiments, accounting for a total of 13 experiments (Table 1). The type and shape of microplastics was chosen to cover a wide range of plastic types (different material densities) and shapes (fragments or fibers). For example PA and PET have been found the most frequent MP in the water column (Choy et al., 2019). In contrast PVC, despite being the third plastic more produced, it is hardly found in suspension in the water column of aquatic environments (Fernández-González et al., 2022).

2.3. Sediment and MP characteristics

The sediment used was Arizona coarse test dust (ISO 12103-1, Powder Technology Inc., Burnsville, USA), which predominantly consists of silica (69–77 %) and aluminum oxide (8–14 %), with a density of 2.65 g/cm^3. Sediment shape was assumed spherical for the calculations since none of the three dimensions prevails over the others. The d_{50} is equal to 35 μm (Fig. 3(A1)). By particle size distribution, they resulted in being poorly sorted (σ = 1.79) (Folk and William Ward, 1957). Three MP were used in the current study: PA and PVC fragments, and PET fibers. PA and PVC fragments were mechanically obtained in the laboratory, then sieved for mesh sizes of 125 μm and 500 μm to sort them into the working range (see the Supplementary Material for more details). The polymer type was measured with IR equipment (Bruker – ALPHA ATR) and compared with known libraries (OPUS Library and Open Specy v0.9.3 (Cowger et al., 2021)) to classify them. The spectrum obtained for each polymer used is presented in the Supplementary Material. Their respective particle size distribution was measured with a laser particle size analyzer (Lisst-100x, Laser In-Situ Scattering and Transmissometry, Sequoia Scientific, Inc., Bellevue, WA) to obtain particle size-distribution (Fig. 3(A2) and (A3)), and the cumulative particle size distributions were determined from the particle size distribution (Fig. 3(B2) and (B3)). The LISST-100X consists of a laser beam and an array of detector rings of progressive diameters which allow the light received at the scattering angles of the beam to be analyzed. The device measures particle volume concentrations for 32 size classes

Table 1
Experimental conditions considered for each run. Sediment concentration considered in the mixing chamber (C_{sed}, in g/l), MP concentration in the mixing chamber (C_{MPs}, in g/l), type of MP (PA = polyamide, PVC = polyvinyl chloride and PET = polyethylene terephthalate). The shape of each type of MP (fragment or fiber) is also included, as well as their density (in kg m^{-3}). The Corey Shape Factor (CSF) of MP particles in each case was calculated by averaging the CSF values of ten particles. For each particle the longest, intermediate, and shortest diameters were measured using an optical microscope (ZEISS SteREO Discovery.V12 - objective PlanApo S 1.5x) equipped with a measuring software (Deltapix InSight v6.5.3 with a Deltapix Invenio 20EIII acquisition camera). The settling velocity was estimated using the formula elaborated by Francalanci et al. (2021). Sediment settling velocity is referenced to d_{50}. ∗Experiment was repeated 3 times to test replicability.

Run #	C_{sed} [g/l]	C_{MPs} [g/l]	MPs type [–]	Shape [–]	Density [g/cm^3]	CSF [–]	Settling velocity [m/s]
1	0	4	PA	Fragment	1.14 ± 0.03	0.45	0.004 ± 0.0008
2	15	4	PA	Fragment	1.14 ± 0.03	0.45	0.004 ± 0.0008
3	30	4	PA	Fragment	1.14 ± 0.03	0.45	0.004 ± 0.0008
4	45	4	PA	Fragment	1.14 ± 0.03	0.45	0.004 ± 0.0008
5	0	4	PVC	Fragment	1.37 ± 0.06	0.32	0.01 ± 0.004
6	15	4	PVC	Fragment	1.37 ± 0.06	0.32	0.01 ± 0.0041
7	30	4	PVC	Fragment	1.37 ± 0.06	0.32	0.01 ± 0.0041
8	45	4	PVC	Fragment	1.37 ± 0.06	0.32	0.01 ± 0.0041
9∗	0	0.05	PET	Fiber	1.38 ± 0.02	0.14	0.006 ± 0.0006
10	15	0.05	PET	Fiber	1.38 ± 0.02	0.14	0.006 ± 0.0006
11	30	0.05	PET	Fiber	1.38 ± 0.02	0.14	0.006 ± 0.0006
12	45	0.05	PET	Fiber	1.38 ± 0.02	0.14	0.006 ± 0.0006
13	30	0	–	–	–	–	0.001

(logarithmically distributed in the size range of 2.5–500.0 μm), using a procedure based on the diffraction theory of light. This instrument has been widely used for measuring both organic (Serra et al., 2001) and inorganic particles (Ros et al., 2014; Serra et al., 2002). The PA and PVC fragments presented d_{50} = 255 μm and d_{50} = 273 μm, respectively (Fig. 3(B2) and (B3)). PET fibers were obtained by cutting 3 mm length fibers of 45 μm thickness from a spool thread. The characteristics of the structure of each MP were observed with an optical microscope (ZEISS SteREO Discovery. V12). Both PA and PVC presented irregular shapes (Fig. 2(a)–(b), respectively). In contrast, PET fibers presented a constant diameter and were more uniform (Fig. 2(c)). To determine the mean thickness of MP, a sectional analysis of the particle was performed through-the-plane for each type of MP (as shown in Fig. 2(d), (e) and (f)) and the maximum length obtained along this section was obtained with the optical microscope (Fig. 2 (g), (h) and (i)).

2.4. Measurement procedure

Samples from the sedimentation traps were transferred into glass beakers, brought to a known volume of 100 ml, and immediately analyzed using one of two different procedures depending on the type of particles. Sediments, PA-fragments, and PVC-fragments were analyzed with the Lisst-100x, but since the fibers were outside of the measurable range of the Lisst-100x, they were counted instead. To count fibers, water samples were transferred into beakers (one for each trap box) and subsequently dried in the oven at 60 °C. Images of fibers in each baker were acquired and analyzed with the ImageJ software to count them. The flume was completely cleaned at the end of each experiment. Water samples were collected in the flume before each experiment and analyzed with the Lisst-100x to ensure the complete removal of MPs particles and sediments from the previous experiment.

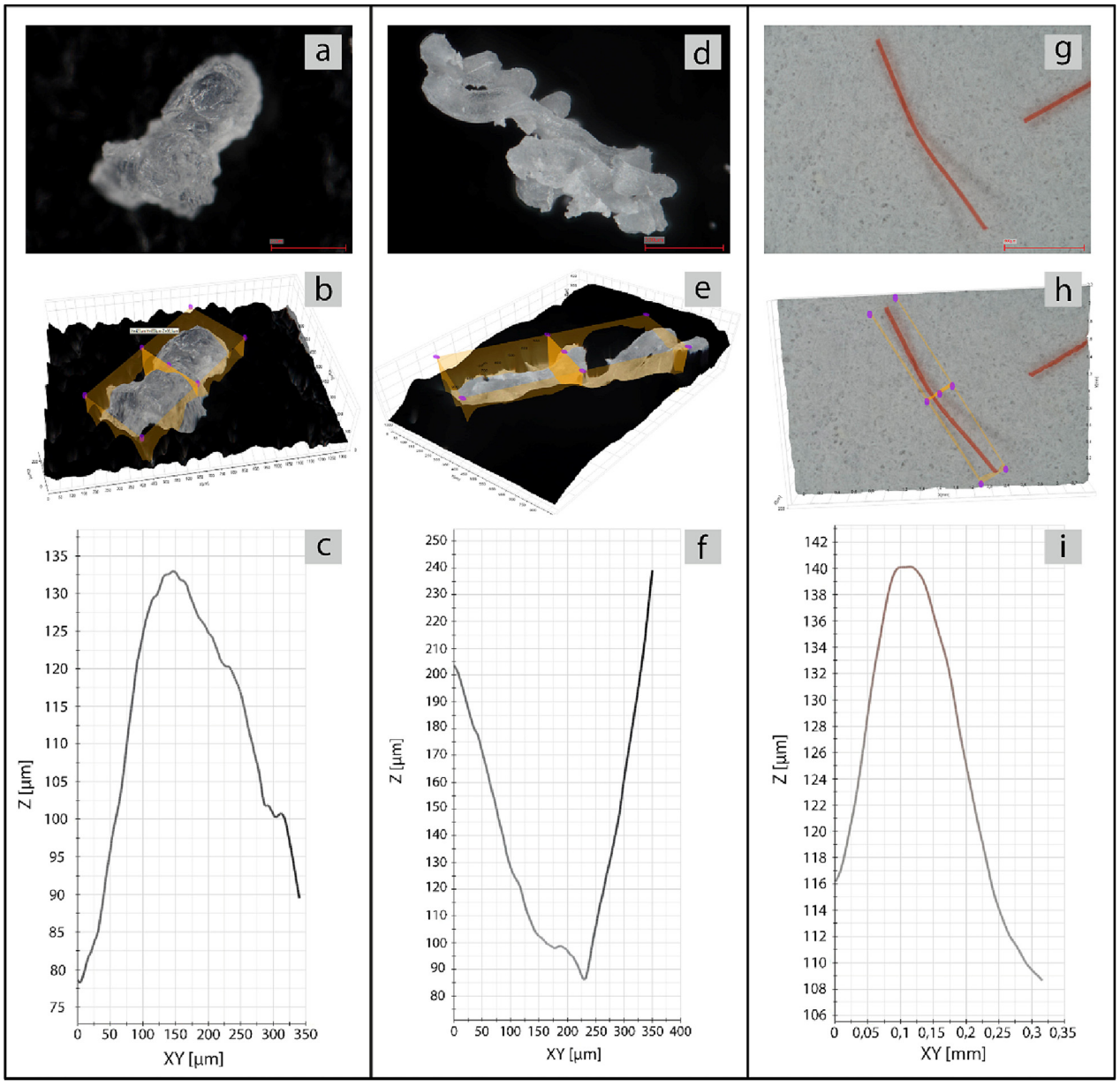

Fig. 2. Geometric characteristics of each type of MP particle considered. Image acquisitions for PA fragments (a), PVC fragments (d) and PET fibers (g) were acquired with an optical microscope (ZEISS SteREO Discovery.V12 - objective PlanApo S 1.5x) equipped with a Deltapix Invenio 20EIII acquisition measuring camera. The 3D-image reconstructions of MP particles (respectively b, e and h) and the measurement of thickness (respectively c, f and i) were obtained with the software Deltapix InSight v6.5.3. Measurements of the thickness were carried out by selecting the most representative sections. All images were captured at 5 Mpx.

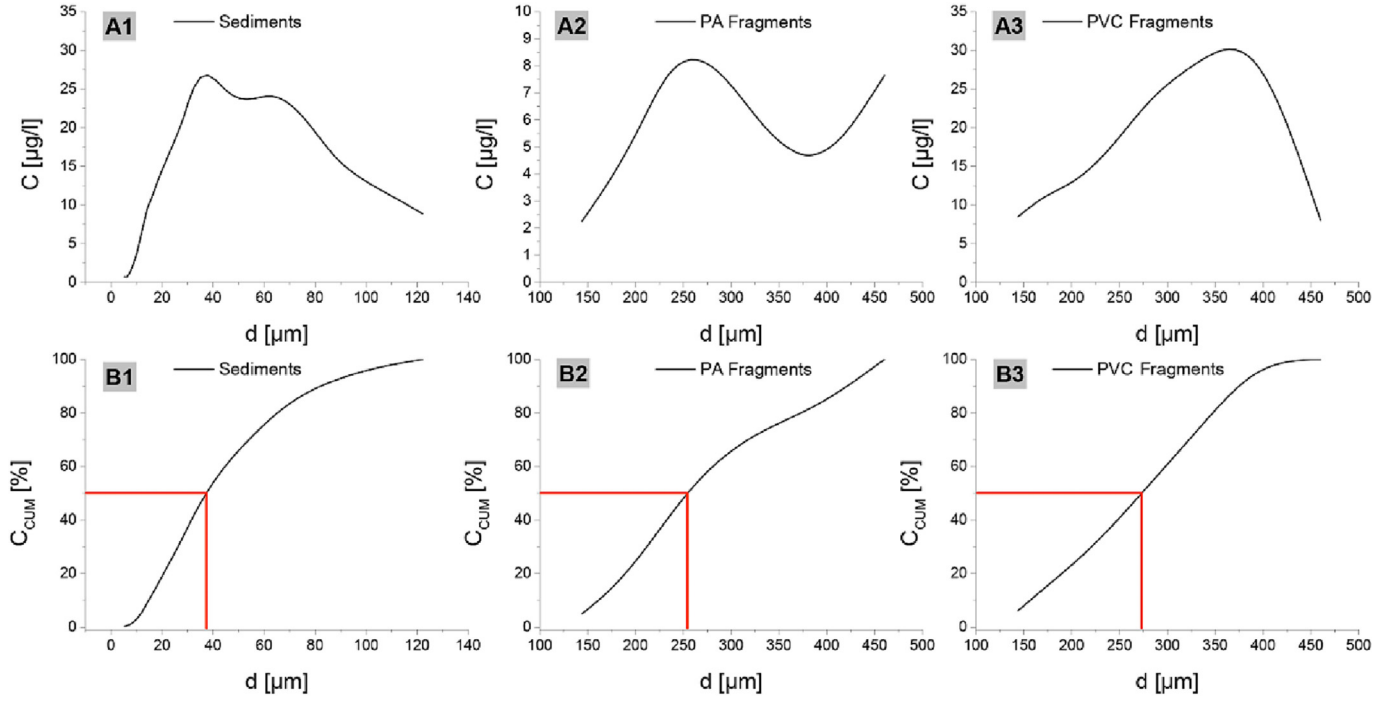

Fig. 3. Particle size distributions (A) and cumulative size curve (C_{CUM}) (B) respectively for sediments (1), PA fragments (2) and PVC fragments (3). Red lines indicate the size corresponding to the d_{50} for each type of particle analyzed. All measurements of the particle concentration (C) were performed by using the Lisst-100x.

2.5. Theory

The dimensional settling velocity (W) was derived from (Francalanci et al., 2021):

$$W = W^{*}\cdot(gRv)^{1/3} \tag{1}$$

where g is the gravity acceleration [m/s^2], ρ and ρ_{MP} are the densities for water and MP, respectively, R is the submerged relative density ($\rho_{MP} - \rho$) / ρ, ν the fluid kinematic viscosity [m^2/s] and W* the dimensionless settling velocity, as provided by Francalanci et al. (2021), and valid for the entire flow regime range. W* can be calculated with the following equation:

$$W^{*} = \frac{D_{*}^{2}}{C_1 + \left(0.75\cdot C_2 \cdot D_{*}^{3}\right)^{n}} \tag{2}$$

where D* is the dimensionless reference diameter defined as follows:

$$D_{*} = D_g \left(\frac{gR}{\nu^2}\right)^{1/2} \tag{3}$$

with D_g = a(CSF)$^{0.34}$(b/a)$^{0.5}$ being the "modified" representative diameter that considers the shape defined by Francalanci et al. (2021), $C_1 = 18E^{-0.38}$ is a dimensionless coefficient dependent on $E = a\left(\frac{a^2+b^2+c^2}{3}\right)^{-1/2}$ and C_2 and n are two dimensionless coefficients dependent on the Corey Shape Factor (CSF = c / $\sqrt{ab}$) and defined as in Eqs. (4) and (5), respectively:

$$C_2 = 0.3708(CSF)^{-0.1602} \tag{4}$$

$$n = 0.4942(CSF)^{-0.059} \tag{5}$$

where a, b and c are the longest, the intermediate, and the shortest axis, respectively, of the measured particles. *CSF* is a dimensionless shape factor representing the relative flatness of the particle where *ab* represents the particle projected area and *c* corresponds to the particle thickness (Albar, 2000). *CSF* ranges from 0 to 1, with the smaller *CSF* the flatter the particle.

To better characterize particle transport along the flume, the Rouse number (P) was calculated using the following formula (Rouse, 1937):

$$P = \frac{W}{k\cdot u_{*}} \tag{6}$$

where W is the dimensional settling velocity defined in Eq. (1), k is the von Karman constant assumed equal to 0.41, u_* is the shear velocity defined as $u\frac{n}{a}\left(gR^{-\frac{1}{3}}\right)^{0.5}$, u is the mean velocity of the flow, a is a dimension correction factor equal to 1 m$^{1/3}$/s, n is the Gauckler–Manning coefficient assumed equal to 0.015, and R is the hydraulic radius of the flume.

Particles settle as they are transported along the flume and volumetric concentration is expected to follow an exponential trend, where C can be written as follows:

$$C = C_{MAX}\cdot e^{-Kx} \tag{7}$$

where C is the particle concentration at distance x, C_{max} is the maximum concentration (near the source), and K is the sedimentation rate (in m^{-1}). From this equation, the characteristic distance reached by each MP (ΔX) can be calculated as the distance where C has decreased e times the maximum concentration C_{MAX}. The sedimentation rate (K) can be determined from the exponential decay of the concentration (C) for each type of MP and for each experiment conducted with different sediment concentrations (C_{sed}).

$$K = -\frac{1}{\Delta x}\ln\left(\frac{C}{C_{MAX}}\right) \tag{8}$$

2.6. Data analysis

The calculation of mean values, the standard error of mean values, the error bars and *p*-values (Fig. 7) were calculated with Microsoft Excel® (Microsoft, US). Pearson correlation coefficients (Fig. 7) and the box plot

showed in Fig. S2 were performed using OriginPro version 9.0 (OriginLab Corp., US). For all statistical analysis the significance level applied was $\alpha = 0.05$.

3. Results

3.1. Characterization of MP and sediment

Both PA and PVC fragments were very irregular in shape, whereas PET fibers were comparable to cylinders with a smooth surface and constant diameter of 45 μm (Fig. 2). PA and PVC fragments were not uniform in size, having a mean equivalent spherical diameter (d_{eq}) of 265.9 ± 29.2 μm and 272.5 ± 72.4 μm, respectively. In contrast, PET fibers were a more uniform size with a mean d_{eq} equal to 191.5 ± 12.4 μm. The lowest Corey Shape Factor (CSF, see Theory section) was found for PET fibers, followed by PVC fragments, and then PA fragments that had the largest CSF among all the particles used in the current study (Table 1).

The settling velocity (W) for each type of MP particle and for sediment particles was calculated following Eq. (1) (see Theory section). The settling velocity for sediment particles ranged between $W = 8.5 \times 10^{-7}$ m/s to 0.06 m/s. For the three size ranges selected (fine/medium silts, coarse silts, and fine sands) in particular, the mean W calculated was $6.77 \cdot 10^{-5}$ m/s, 0.001 m/s and 0.009 m/s, respectively. W for sediments at d_{50} was 0.001 m/s. For MP W were 0.0040 ± 0.0008 m/s, 0.010 ± 0.004 m/s and 0.0060 ± 0.0006 m/s for PA fragments, PVC fragments, and PET fibers, respectively (Fig. S2, Table 1). The Rouse numbers for the three sediment size ranges were calculated following Eq. (6) (see Theory section). The Rouse number resulted in being equal to 0.16 ± 0.02 (corresponding to the wash load mode of transport) for the fine/medium silts, 2.39 ± 0.41 (corresponding to the suspended load/bed load mode of transport) for the coarse silts, and 21.53 ± 3.70 (corresponding to the bed load mode of transport) for the fine sand.

3.2. Transport of sediment along the flume

The normalized sediment concentration (C_{sed}/C_{S_MAX}, where $C_{s\text{-}MAX}$ was the maximum concentration of sediment found near the source) decreased along the flume at a decay rate that went from an approximately linear trend for the fine/medium silt range, and then followed exponential trends for the Coarse silt (CS) and the Fine sand (FS) ranges. In addition, C_{sed}/C_{S_MAX} decreased as the size range increased (Fig. 4(a)). No differences were observed for the decrease of C_{sed}/C_{S_MAX} along the flume for the experiments carried out with different sediment concentrations and a mean standard deviation (σ_M) equal to 0.05 (Fig. 4(b)). For each experiment, and for each sediment size range, a value of at least C_{sed}/C_{S_MAX} equal to 0.10 was registered at the end of the shallow zone (a minimum value of $C_{sed}/C_{S\_MAX} = 0.15$ was also found).

The normalized concentration of MP ($C/C_{MP\text{-}MAX}$) decreased along the flume following an exponential trend in all the experiments conducted, independent of whether experiments were carried out with or without sediment (Fig. 5). For the experiments carried out without sediment, the decay rates of MP depended on the type of MP considered, with the greatest rate of decrease being for PVC fragments and the lowest for PA fragments. Fibers presented a rate of decrease between PVC and PA fragments (Fig. 5 (a)). In the experiments carried out with sediment, the rate of decay of MP also depended on the presence of suspended sediment (Fig. 5(b)). In this case, PA and PVC presented a greater rate of sedimentation along the x axis than fibers. In the case with sediments, PA presented a greater decay than in the experiments carried out without sediments. In contrast, PVC presented similar rates of decay for experiments carried out with sediments compared to those carried out without sediments. For the case of fibers, $C/C_{MP\text{-}MAX}$ decreased more rapidly with the progressive distance in the case without sediment than for the case with sediment. Sediments also presented an exponential decay rate, with the smaller sediment particles (coarse silts, Fig. 5(b)) presenting a slower decay rate than the largest sediment particles considered (fine sands, Fig. 5(b)).

For all the MP investigated, the rate of decay along the x axis increased as C_{sed} in the mixing chamber increased (see Fig. 6(a)–(c)). However, the rate of decay of MP for the different C_{sed} depended on the type of MP. PA fragments presented a gradual increase in the rate of decay as C_{sed} increased (Fig. 6(a)), whereas PVC fragments presented a slight change with C_{sed} (Fig. 6(b)). However, fibers presented a behavior with C_{sed} that fell between that observed for PVC and PET fragments (Fig. 6(c)).

The characteristic distance along x up to where each type of MP was transported (ΔX) decreased as C_{sed} increased and ranged from 77 cm to 196 cm in the case of PA fragments, and from 63 cm to 72.5 cm in the case of PVC fragments (Fig. 6(a), (b)). For PET fibers, for $C_{sed} = 15$ g/l, $C_{sed} = 30$ g/l and $C_{sed} = 45$ g/l, ΔX decreased from 153 cm to 99.5 cm. For $C_{sed} = 0$ g/l, $\Delta X = 122$ cm. The sedimentation rate (K, in cm^{-1}) was calculated with Eq. (8) and plotted in Fig. 7. K presented the highest values for PVC fragments, followed by PA fragments, and then PET fibers. For all particle types, K increased linearly with the sediment concentration

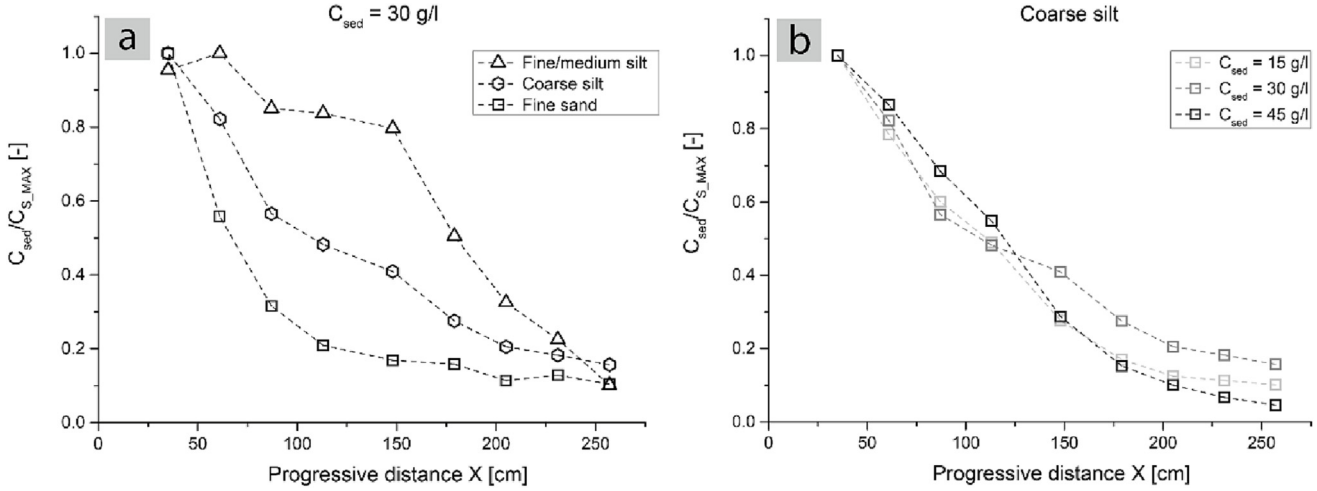

Fig. 4. (a): Horizontal profiles of the normalized concentrations (C_{sed}/C_{S_MAX}) for the three sediments size ranges identified along the flume for the case of Csed = 30 g/l. Each measuring point on the graphs has been derived from the average of the MP concentrations measured in each sampling point (Fig. 1). (b): Horizontal profiles of the normalized concentration (C_{sed}/C_{S_MAX}) of the coarse silt along the flume to vary C_{sed}. Each measuring point on the graphs has been derived from the average of the MP concentrations measured in each sampling point.

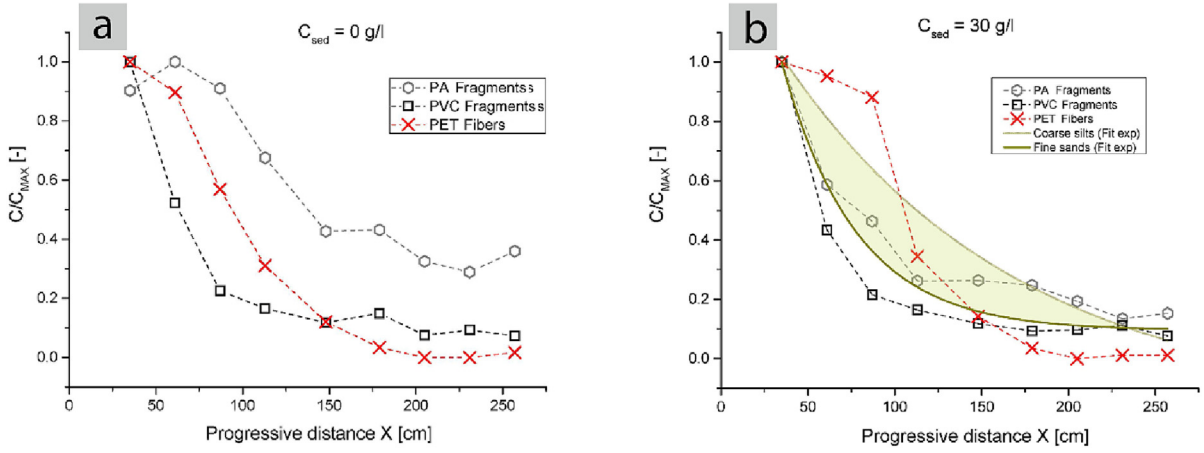

Fig. 5. Horizontal profiles of the normalized concentration of MPs (C/C_{MAX}) along the flume for the case of C_{sed} = 0 g/l (a) and C_{sed} = 30 g/l (b). Each measuring point on the graphs is derived from the average of the MP concentrations measured in the two sediment traps situated at each measuring position x. The initial measuring point (x = 0 cm) corresponds to Section C (Fig. 1), which is also the injection point for both sediments and MP. The green shaded area in (b) represents the range of sediment distribution for the different sediment sizes. The upper limit of the green area corresponds to the distribution of finer sediment particles (coarse silts) and the lower limit of the green area corresponds to the coarser sediment particles considered (fine sands).

(C_{sed}), except for the experiment of fibers without sediment (Fig. 7). The slopes of the linear trends depended on the MP type.

4. Discussion

4.1. MP scavenging by sediment particles under unidirectional flows

The current study determined the effect sediments have on the vertical and horizontal transport of MP in shallow water systems dominated by a unidirectional current. In natural environments, MP may be suspended in the water column and can interact with other particles (organic or inorganic) that are suspended in the water column (Liu et al., 2022). Without any physical forcing, i.e., under very calm conditions, sediment particles have been found to increase the settling rate of MP in the water column (Li et al., 2019).

The current study demonstrates that sediment particles increase the transport of MP to the bottom under a unidirectional flow regime. Under these conditions, the concentration of MP decreased exponentially with distance with a decay rate that depended on the type of MP. This study aligns with the findings of Pohl et al. (2020), who found that sediment particles enhance the downward vertical transport of MP in gravity current processes, providing a hypothesis on why MP can accumulate and be buried in marine bed sediments (Leiser et al., 2021). In addition, the current study demonstrates that sediment concentration also played a crucial role in the transport of MP along the flume, with greater sedimentation of MP to the bottom as sediment concentration increased. Serra and Colomer (2023) compared MP scavenging by sediment particles in sheared settings (pure turbulence generated by an oscillating grid) to calm conditions. Sediment increased the vertical flux of MP to the bed, meanwhile the shear resuspended MP and sediments. Therefore, the greater the shear the greater the concentration of MP in suspension. Therefore, hydrodynamics impact on the vertical flux of MP. Different hydrodynamics are expected to impact differently on the behavior of MP in the water column. In this case, a unidirectional current is expected to produce a shear in the water column and therefore impact on the sedimentation rate in the water column, reducing the flux of particles to the bottom when compared to calm conditions.

4.2. Scavenging of different types and shapes of MP by sediment particles

The settling velocities of MP particles depended on the density of each polymer type, as also found by others (Elagami et al., 2022; Li et al., 2019). However, in the current study, not only their density was found to be the main parameter but so too their shapes and equivalent diameters (Table 1), in accordance with Waldschläger and Schüttrumpf (2020). In all the experiments, the highest rate of decay was for PVC, the second for PA fragments and the lowest for PET fibers. This was attributed to the settling velocity of each type of particle (Fig. S2, Table 1): PVC fragments

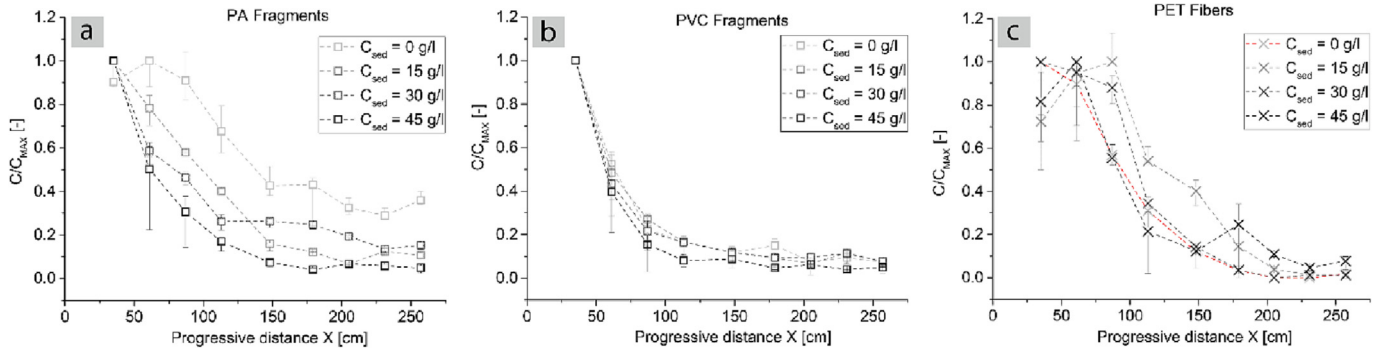

Fig. 6. Horizontal profiles of the normalized concentration ($C/C_{s\text{-}MAX}$) of the MPs along the flume to vary C_{sed} for the case of PA fragments (a), PVC fragments (b), PET fibers (c). Each measuring point on the graphs is derived from the average of the MP concentrations measured in the two box traps located in each measuring section. The initial measuring point (x = 0 cm) corresponds to Section C (see Fig. 1(a)), which is also the injection point for both sediments and MP. Error bars were calculated for each measurement section considering the maximum and minimum C value measured and then taking the deviation from the mean value.

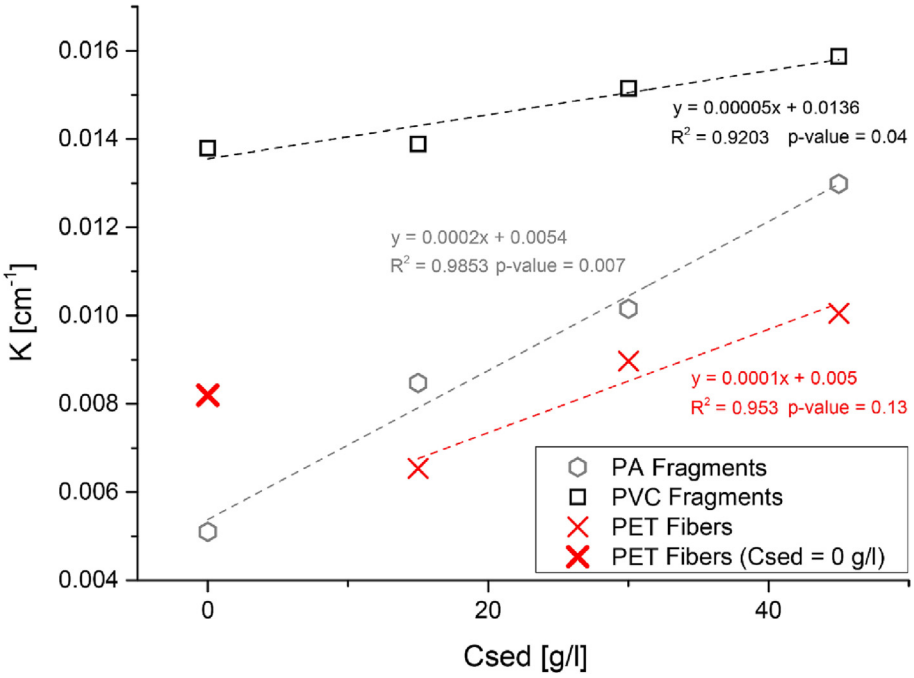

Fig. 7. Sedimentation rate (K) for the different types of MP particles analyzed. The isolated red cross in bold represents K in the case of the without sediments setup. A one-way ANOVA test for the K obtained for different MP showed that the sedimentation rate for each MP particle (PA fragments, PVC fragments and PET fibers) is significantly different (*p*-value = 0.01).

had the highest settling velocity followed by PA-fragments and then by PET-fibers.

The decay rate of MP increased with the sediment concentration for all the MP studied but with different intensities. The greatest increase in the decay rate was for PA fragments followed by fibers and PVC. The increments were 154.9 %, 22.0 % and 8.7 %, respectively, when comparing the decay rate for C_{sed} = 0 g/l with C_{sed} = 45 g/l. The change in the decay rates was attributed to sediments that have a greater settling velocity than MP (Table 1). Therefore, fast settling sediment particles scavenged suspended low settling PA fragments, thus increasing their transport along the water column. The greater the suspended sediment concentration, the greater the number of PA fragments being transported downwards. In contrast, PVC fragments had the greatest settling velocity, close to that of sediment particles. In this case, the increase in the sediment concentration caused a small effect on the vertical transport of MP of PVC. It must be noticed that for the case without sediment, fibers presented a greater decrease rate than that for C_{sed} = 15 g/l. This was attributed to the fact that fibers may remain suspended in the water column while they are advected, thus having little settling along the flume. Indeed, shape is a fundamental parameter on the settling process of MP particles. Fibers settle with their long axis perpendicular to the direction of the fall, exposing a larger surface in relation to the volume to the floating force (Khatmullina and Isachenko, 2017), presenting a low settling rate without suspended sediments, and a substantial number of them reached the end of the platform before reaching the bottom, as confirmed by visual observation. When sediment was added, sediment particles scavenged fibers, thus increasing their settling. Li et al. (2019) did not find an increase in the settling rate of floating MP due to the presence of sediment particles. However, the shear produced by advection in the current study might mediate the sediment/fiber interaction, making it possible for them to be transported to the bottom of the flume. Sediment particles situated above fibers will scavenge MP towards the bottom, so the depositional functioning should have a greater effect on particles that exhibit a greater surface area in the direction perpendicular to the sinking; as already noted by Pohl et al. (2020) in the case of MP transported by turbidity currents.

Additionally, it should be noted that the sedimentation rate for the case of PA fragments was more affected by the different concentrations of suspended sediment than for the case PVC fragments. This can be attributed to the fact that the calculated settling velocity for the PA fragments is different to that of the d_{50} of the sediment (Fig. S2). This mechanism has already been observed for other types of particles, particularly metals (Liu et al., 2019).

In contrast, PVC fragments have rapid sinking rates, close to sediment particles (Table 1), and therefore their vertical transport is less affected by settling sediment particles compared to the other two MP studied. Consequently, similar sinking processes between particles might explain why the accumulation of MP at the bottom of sediment beds has a direct relationship with the sinking rates of sediment particles in aquatic ecosystems. This result is in agreement with the observations of the percentages of MP and sediments that were found to accumulate at the bottom of the water column in the Venice Lagoon (Vianello et al., 2013).

The current study demonstrates that the vertical transport of MP along a system will depend on the type of MP and the sediment concentration interacting with the MP particles in the driving unidirectional flow. Therefore, the greater the settling rate of MP is, the shorter the horizontal distance traveled by the different MP particles, which consequently accumulate at different distances from the source. This result agrees with He et al. (2021) who stated that rivers acted as MPS sinks rather than transport pathways. However, the current study has demonstrated that a slow sinking MP that would be expected to travel longer distances, is mediated by sediment dynamics. In this case, the greater the sediment concentration, the greater the sinking rate of MP to the bottom. Therefore, the MP sedimentation patterns may present a segregated distribution in riverbeds in response to the mediation of suspended sediments on the MP sedimentation.

Elagami et al. (2022) studied the transport of MP in the water column of a lake and found that slow settling MP particles (i.e., those with long residence times in the water column) would be unlikely to settle to the lake sediment. However, the current study has proved that MP can be scavenged by fast settling sediment particles, thus increasing their sedimentation rates. This process can be added to other mechanisms such as adsorption, aggregation, and biofouling that explain the high concentration of low-density MP found in wetlands bed load sediments (Badylak et al., 2021; Dalvand and Hamidian, 2023; Rasta et al., 2020). Therefore, MP scavenging by sediment should be regarded as one of the main, not secondary, mechanisms

that fuel MP sedimentation. Finally, MP located at different water depths show different degrees of weathering from solar irradiation, biological degradation, mechanical wearing, and pyrolysis, which results in different mass losses or degradation rates (Alimi et al., 2018). Consequently, faster MP sinking rates, because of scavenging, could lead to an extension in the degradation times of the MP, thus also impacting their particle size distribution in the environment.

5. Conclusion

In the current study, the longitudinal transport of MP particles from a particle-laden plume was found to not only depend on the type of MP, but also on the fact that fast settling sediment particles scavenged MP particles, thus increasing their settling rates. Therefore, the current study demonstrates that there is a heterogeneous distribution of MP and that the sedimentation patterns of the different MP types segregate them as they are transported. This indicates that fast sinking MP will not be transported far from their source before they accumulate in the ecosystem sediment bed. In contrast, slow settling MPs can travel further, but this will depend on the concentration of suspended sediment in the particle-laden plume. Thus, their extension will decrease as the sediment concentration increases. In the case of PA fragments, the rate of sedimentation increased by 154.9 % when the sediment concentration increased from 0 g/l to 45 g/l. The sedimentation rate of PET fibers and PVC increased by 22.0 % and 8.7 %, respectively, below that obtained for PA. This indicates that the distance traveled by MP from the contaminant sources would be greatly reduced when MP are transported with sediment particles. Therefore, results confirm the hypothesis of stated in the current manuscript.

The findings during this work, and the implications discussed above, indicate the importance of taking suspended sediment concentration into account as an additional fundamental parameter in the development of new MP transport models in low-energy aquatic environments, due to the capacity of suspended sediment to significantly modify the mass balance of plastic particles discharged into aquatic ecosystems.

CRediT authorship contribution statement

Mirco Mancini: Methodology, Software, Formal analysis, Investigation, Writing – original draft, Writing – review & editing, Visualization. **Teresa Serra:** Conceptualization, Methodology, Validation, Resources, Writing – original draft, Writing – review & editing, Visualization, Supervision, Funding acquisition. **Jordi Colomer:** Conceptualization, Methodology, Validation, Resources, Writing – original draft, Writing – review & editing, Visualization, Supervision, Funding acquisition. **Luca Solari:** Conceptualization, Validation, Writing – original draft, Writing – review & editing, Visualization, Supervision.

Data availability

Data will be made available on request.

Declaration of competing interest

The authors declare that they have no known competing financial interests or personal relationships that could have appeared to influence the work reported in this paper.

Acknowledgments

This work was supported by the Ministerio de Economía y Competitividad of the Spanish Government through Grant PID2021-123860OB-I00. We are grateful to the University of Girona Research Technical Services and also to the Grup de Recerca en Materials i Termodinàmica of the University of Girona for all the technical assistance provided to develop this project. We also thank Pere Bellvehí for all the technical help provided.

Appendix A. Supplementary data

Supplementary data to this article can be found online at https://doi.org/10.1016/j.scitotenv.2023.164363.

References

Albar, A., 2000. Effect of various terminal velocity equations on the result of friction loss calculation. Terra et Aqua81 pp. 13–21.
Alimi, O.S., Farner Budarz, J., Hernandez, L.M., Tufenkji, N., 2018. Microplastics and nanoplastics in aquatic environments: aggregation, deposition, and enhanced contaminant transport. Environ. Sci. Technol. 52 (4), 1704–1724. https://doi.org/10.1021/acs.est.7b05559.
Badylak, S., Phlips, E., Batich, C., Jackson, M., Wachnicka, A., 2021. Polystyrene microplastic contamination versus microplankton abundances in two lagoons of the Florida Keys. Sci. Rep. 11, 6029. https://doi.org/10.1038/s41598-021-85388-y.
Bakhteeva, I.A., Medvedeva, I.V., Filinkova, M.S., Byzov, I.V., Minin, A.S., Zhakov, S.V., Uimin, M.A., Patrakov, E.I., Novikov, S.I., Suntsov, A.Yu., Demin, A.M., 2023. Removal of microplastics from water by using magnetic sedimentation. Int. J. Environ. Sci. Technol. https://doi.org/10.1007/s13762-023-04776-1.
Ballent, A., Pando, S., Purser, A., Juliano, M.F., Thomsen, L., 2013. Modelled transport of benthic marine microplastic pollution in the Nazaré Canyon. Biogeosciences 10 (12), 7957–7970. https://doi.org/10.5194/bg-10-7957-2013.
Bergmann, M., Gutow, L., Klages, M., 2015. Marine Anthropogenic Litter. Springer, pp. 1–447 https://doi.org/10.1007/978-3-319-16510-3.
Besseling, E., Quik, J.T.K., Sun, M., Koelmans, A.A., 2017. Fate of nano- and microplastic in freshwater systems: a modeling study. Environ. Pollut. 220, 540–548. https://doi.org/10.1016/j.envpol.2016.10.001.
Colomer, J., Müller, M.F., Barcelona, A., Serra, T., 2019. Mediated food and hydrodynamics on the ingestion of microplastics by Daphnia magna. Environ. Pollut. 251, 434–441. https://doi.org/10.1016/j.envpol.2019.05.034.
Cowger, W., Steinmetz, Z., Gray, A., Munno, K., Lynch, J., Hapich, H., Primpke, S., de Frond, H., Rochman, C., Herodotou, O., 2021. Microplastic spectral classification needs an open source community: open specy to the rescue! Anal. Chem. 93 (21), 7543–7548. https://doi.org/10.1021/acs.analchem.1c00123.
Critchell, K., Lambrechts, J., 2016. Modelling accumulation of marine plastics in the coastal zone; what are the dominant physical processes? Estuar. Coast. Shelf Sci. 171, 111–122. https://doi.org/10.1016/j.ecss.2016.01.036.
Dalvand, M., Hamidian, A.H., 2023. Occurrence and distribution of microplastics in wetlands. Sci. Total Environ. 862, 160740. https://doi.org/10.1016/j.scitotenv.2022.160740.
de Klein, J.J.M., Quik, J.T.K., Bäuerlein, P.S., Koelmans, A.A., 2016. Towards validation of the NanoDUFLOW nanoparticle fate model for the river Dommel, the Netherlands. Environ. Sci. Nano 3 (2), 434–441. https://doi.org/10.1039/c5en00270b.
Dietrich, W.E., 1982. Settling velocity of natural particles. Water Resour. Res. 18 (6), 1615–1626. https://doi.org/10.1029/WR018i006p01615.
Elagami, H., Ahmadi, P., Fleckenstein, J.H., Frei, S., Obst, M., Agarwal, S., Gilfedder, B.S., 2022. Measurement of microplastic settling velocities and implications for residence times in thermally stratified lakes. Limnol. Oceanogr. 67 (4), 934–945. https://doi.org/10.1002/lno.12046.
Fernández-González, V., Andrade-Garda, J.M., López-María, P., Muniategui-Lorenzo, S., 2022. Misidentification of PVC microplastics in marine environmental samples. TrAC Trends Anal. Chem. 153, 116649. https://doi.org/10.1016/j.trac.2022.116649.
Folk, R.L., William Ward, X.C., 1957. Brazos River bar: a study in the significance of grain size parameters. J. Sedimentary Petrol. 27 (1), 3–26.
Francalanci, S., Paris, E., Solari, L., 2021. On the prediction of settling velocity for plastic particles of different shapes. Environ. Pollut. 290 (1), 118068. https://doi.org/10.1016/j.envpol.2021.118068.
Geyer, R., Jambeck, J.R., Law, K.L., 2017. Production, use, and fate of all plastics ever made. Sci. Adv. 3 (7), e1700872. https://doi.org/10.1126/sciadv.1700782.
He, B., Smith, M., Egodawatta, P., Ayoko, G.A., Rintoul, L., Goonetilleke, A., 2021. Dispersal and transport of microplastics in river sediments. Environ. Pollut. 279, 116884. https://doi.org/10.1016/j.envpol.2021.116884.
Helcoski, R., Yonkos, L.T., Sanchez, A., Baldwin, A.H., 2020. Wetland soil microplastics are negatively related to vegetation cover and stem density. Environ. Pollut. 256, 113391. https://doi.org/10.1016/j.envpol.2019.113391.
Hidalgo-Ruz, V., Gutow, L., Thompson, R.C., Thiel, M., 2012. Microplastics in the marine environment: a review of the methods used for identification and quantification. Environ. Sci. Technol. 46 (6), 3060–3075. https://doi.org/10.1021/es2031505.
Huang, W., Song, B., Liang, J., Niu, Q., Zeng, G., Shen, M., Deng, J., Luo, Y., Wen, X., Zhang, Y., 2021. Microplastics and associated contaminants in the aquatic environment: a review on their ecotoxicological effects, trophic transfer, and potential impacts to human health. J. Hazard. Mater. 405, 124187. https://doi.org/10.1016/j.jhazmat.2020.124187.
Ivar Do Sul, J.A., Costa, M.F., 2014. The present and future of microplastic pollution in the marine environment. Environ. Pollut. 185, 352–364. https://doi.org/10.1016/j.envpol.2013.10.036.
Keddy, P., 2010. Wetland Ecology: Principles and Conservation. 2nd edition. Cambridge University Press.
Khatmullina, L., Isachenko, I., 2017. Settling velocity of microplastic particles of regular shapes. Mar. Pollut. Bull. 114 (2), 871–880. https://doi.org/10.1016/j.marpolbul.2016.11.024.
Kumar, R., Sharma, P., Verma, A., Jha, P.K., Singh, P., Gupta, P.K., Chandra, R., Vara Prasad, P.V., 2021. Effect of physical characteristics and hydrodynamic conditions on transport and deposition of microplastics in riverine ecosystem. Water 13 (19), 2710. https://doi.org/10.3390/w13192710.

Lagarde, F., Olivier, O., Zanella, M., Daniel, P., Hiard, S., Caruso, A., 2016. Microplastic interactions with freshwater microalgae: hetero-aggregation and changes in plastic density appear strongly dependent on polymer type. Environ. Pollut. 215, 331–339. https://doi.org/10.1016/j.envpol.2016.05.006.

Leiser, R., Schumann, M., Dadi, T., Wendt-Potthoff, K., 2021. Burial of microplastics in freshwater sediments facilitated by iron-organo flocs. Sci. Rep. 11 (1), 24072. https://doi.org/10.1038/s41598-021-02748-4.

Li, Y., Wang, X., Fu, W., Xia, X., Liu, C., Min, J., Zhang, W., Crittenden, J.C., 2019. Interactions between nano/micro plastics and suspended sediment in water: implications on aggregation and settling. Water Res. 161, 486–495. https://doi.org/10.1016/j.watres.2019.06.018.

Liu, J., Song, J., Yuan, H., Li, X., Li, N., Duan, L., 2019. Trace metal comparative analysis of sinking particles and sediments from a coastal environment of the Jiaozhou Bay, North China: influence from sediment resuspension. Chemosphere 232, 315–326. https://doi.org/10.1016/j.chemosphere.2019.05.090.

Liu, S., Huang, Y., Luo, D., Wang, X., Wang, Z., Ji, X., Chen, Z., Dahlgren, R.A., Zhang, M., Shang, X., 2022. Integrated effects of polymer type, size and shape on the sinking dynamics of biofouled microplastics. Water Res. 220, 118656. https://doi.org/10.1016/j.watres.2022.118656.

Meijer, L.J.J., Van Emmerik, T., Van Der Ent, R., Schmidt, C., Lebreton, L., 2021. More than 1000 rivers account for 80% of global riverine plastic emissions into the ocean. Sci. Adv. 7 (18), eaaz5803. https://doi.org/10.1126/sciadv.aaz5803.

Murphy, S., Voulgaris, G., 2006. Identifying the role of tides, rainfall and seasonality in marsh sedimentation using long-term suspended sediment concentration data. Mar. Geol. 227 (1–2), 31–50. https://doi.org/10.1016/j.margeo.2005.10.006.

Nepf, H.M., Sullivan, J.A., Zavitoski, R.A., 1997. A model for diffusion within emergent vegetation. Limnol. Oceanogr. 42 (8), 1735–1745. https://doi.org/10.4319/lo.1997.42.8.1735.

Ouyang, X., Duarte, C.M., Cheung, S.G., Tam, N.F.Y., Cannicci, S., Martin, C., Lo, H.S., Lee, S.Y., 2022. Fate and effects of macro- and microplastics in coastal wetlands. Environ. Sci. Technol. 56 (4), 2386–2397. https://doi.org/10.1021/acs.est.1c06732.

Pinheiro, L.M., Britz, L.M.K., Agostini, V.O., Pérez-Parada, A., García-Rodríguez, F., Galloway, T.S., Pinho, G.L.L., 2022. Salt marshes as the final watershed fate for meso- and microplastic contamination: a case study from southern Brazil. Sci. Total Environ. 838, 156077. https://doi.org/10.1016/j.scitotenv.2022.156077.

Pohl, F., Eggenhuisen, J.T., Kane, I.A., Clare, M.A., 2020. Transport and burial of microplastics in deep-marine sediments by turbidity currents. Environ. Sci. Technol. 54 (7), 4180–4189. https://doi.org/10.1021/acs.est.9b07527.

Rahmani, M., Gupta, A., Jofre, L., 2022. Aggregation of microplastic and biogenic particles in upper-ocean turbulence. Int. J. Multiphase Flow 157, 104253. https://doi.org/10.1016/j.ijmultiphaseflow.2022.104253.

Rasta, M., Sattari, M., Taleshi, M.S., Namin, J.I., 2020. Identification and distribution of microplastics in the sediments and surface waters of Anzali Wetland in the Southwest Caspian Sea, Northern Iran. Mar. Pollut. Bull. 160, 111541. https://doi.org/10.1016/j.marpolbul.2020.111541.

Ros, À., Colomer, J., Serra, T., Pujol, D., Soler, M., Casamitjana, X., 2014. Experimental observations on sediment resuspension within submerged model canopies under oscillatory flow. Cont. Shelf Res. 91, 220–231. https://doi.org/10.1016/j.csr.2014.10.004.

Rouse, H., 1937. Modern conceptions of mechanics of fluid turbulence. Trans. Am. Soc. Civil Eng. 102, 463–505.

Sanchez-Vidal, A., Canals, M., de Haan, W.P., Romero, J., Veny, M., 2021. Seagrasses provide a novel ecosystem service by trapping marine plastics. Sci. Rep. 11, 254. https://doi.org/10.1038/s41598-020-79370-3.

Schmidt, N., Thibault, D., Galgani, F., Paluselli, A., Sempéré, R., 2018. Occurrence of microplastics in surface waters of the Gulf of Lion (NW Mediterranean Sea). Prog. Oceanogr. 163, 214–220. https://doi.org/10.1016/j.pocean.2017.11.010.

Serra, T., Colomer, J., 2023. Scavenging of polystyrene microplastics by sediment particles in both turbulent and calm aquatic environments. Sci. Total Environ. 884, 163720. https://doi.org/10.1016/j.scitotenv.2023.163720.

Serra, T., Colomer, J., Cristina, X.P., Vila, X., Arellano, J.B., Casamitjana, X., 2001. Evaluation of laser in situ scattering instrument for measuring concentration of phytoplankton, purple sulfur bacteria, and suspended inorganic sediments in lakes. J. Environ. Eng. 127 (11), 1023–1030. https://doi.org/10.1061/(asce)0733-9372(2001)127:11(1023).

Serra, T., Colomer, J., Gacia, E., Soler, M., Casamitjana, X., 2002. Effects of a turbid hydrothermal plume on the sedimentation rates in a karstic lake. Geophys. Res. Lett. 29 (21), 2029. https://doi.org/10.1029/2002GL015368.

Siegfried, M., Koelmans, A.A., Besseling, E., Kroeze, C., 2017. Export of microplastics from land to sea. A modelling approach. Water Res. 127, 249–257. https://doi.org/10.1016/j.watres.2017.10.011.

Smoak, J.M., Breithaupt, J.L., Smith, T.J., Sanders, C.J., 2013. Sediment accretion and organic carbon burial relative to sea-level rise and storm events in two mangrove forests in Everglades National Park. Catena 104, 58–66. https://doi.org/10.1016/j.catena.2012.10.009.

Streit-Bianchi, M., Cimadevila, M., Trettnak, W., 2020. Mare Plasticum-the Plastic Sea. Combatting Plastic Pollution Through Science and Art. Springer, Cham https://doi.org/10.1007/978-3-030-38945-1.

Sun, J., Zheng, H., Xiang, H., Fan, J., Jiang, H., 2022. The surface degradation and release of microplastics from plastic films studied by UV radiation and mechanical abrasion. Sci. Total Environ. 838, 156369. https://doi.org/10.1016/j.scitotenv.2022.156369.

van Cauwenberghe, L., Vanreusel, A., Mees, J., Janssen, C.R., 2013. Microplastic pollution in deep-sea sediments. Environ. Pollut. 182, 495–499. https://doi.org/10.1016/j.envpol.2013.08.013.

van Emmerik, T., Strady, E., Kieu-Le, T.C., Nguyen, L., Gratiot, N., 2019. Seasonality of riverine macroplastic transport. Sci. Rep. 9, 13549. https://doi.org/10.1038/s41598-019-50096-1.

van Emmerik, T., Mellink, Y., Hauk, R., Waldschläger, K., Schreyers, L., 2022. Rivers as plastic reservoirs. Front. Water 3, 786936. https://doi.org/10.3389/frwa.2021.786936.

Vianello, A., Boldrin, A., Guerriero, P., Moschino, V., Rella, R., Sturaro, A., Da Ros, L., 2013. Microplastic particles in sediments of Lagoon of Venice, Italy: first observations on occurrence, spatial patterns and identification. Estuar. Coast. Shelf Sci. 130, 54–61. https://doi.org/10.1016/j.ecss.2013.03.022.

Wagner, M., Lambert, S., 2018. Freshwater microplastics. Handb. Environ. Chem. 58, 302. https://doi.org/10.1007/978-3-319-61615-5.

Waldschläger, K., Schüttrumpf, H., 2020. Infiltration behavior of microplastic particles with different densities, sizes, and shapes-from glass spheres to natural sediments. Environ. Sci. Technol. 54 (15), 9366–9373. https://doi.org/10.1021/acs.est.0c01722.

Wang, X., Bolan, N., Tsang, D.C.W., Sarkar, B., Bradney, L., Li, Y., 2021. A review of microplastics aggregation in aquatic environment: influence factors, analytical methods, and environmental implications. J. Hazard. Mater. 402, 123496. https://doi.org/10.1016/j.jhazmat.2020.123496.

Wang, Y., Chen, X., Wang, F., Cheng, N., 2023. Influence of typical clay minerals on aggregation and settling of pristine and aged polyethylene microplastics. Environ. Pollut. 316, 120649. https://doi.org/10.1016/j.envpol.2022.120649.

Woodall, L.C., Sanchez-Vidal, A., Canals, M., Paterson, G.L.J., Coppock, R., Sleight, V., Calafat, A., Rogers, A.D., Narayanaswamy, B.E., Thompson, R.C., 2014. The deep sea is a major sink for microplastic debris. R. Soc. Open Sci. 1 (4), 140317. https://doi.org/10.1098/rsos.140317.

Yan, Y., Zhu, F., Zhu, C., Chen, Z., Liu, S., Wang, C., Gu, C., 2021. Dibutyl phthalate release from polyvinyl chloride microplastics: influence of plastic properties and environmental factors. Water Res. 204, 117597. https://doi.org/10.1016/j.watres.2021.117597.

Zhao, S., Wang, T., Zhu, L., Xu, P., Wang, X., Gao, L., Li, D., 2019. Analysis of suspended microplastics in the Changjiang Estuary: implications for riverine plastic load to the ocean. Water Res. 161, 560–569. https://doi.org/10.1016/j.watres.2019.06.019.